Universal Journal of Lasers, Optics, Photonics & Sensors (UJLOPS)
UINUJLOPS005/ Yang Xin
ETEXT

Order Analysis Comparison between traditional Fourier Transform-based atmospheric turbulencecompensation methods and new Well Optimized Linear Finder Methodology

Yang Xin, William W. Arrasmith, PhD and Erlin He
Department Of Computer Engineering And Sciences, Florida Institute of Technology
150 W University Blvd, Melbourne, Florida 32901, USA
yxin2012@my.fit.edu, warrasmi@fit.edu, and ehe2011@my.fit.edu

Received: 4 June 2021; **Accepted:** 20 June 2021; **Published**: 21 June 2021

Citation: Yang Xin, William W. Arrasmith, PhD and Erlin He -Order Analysis Comparison between traditional Fourier Transform-based atmospheric turbulence compensation methods and new Well Optimized Linear Finder Methodology (2021): 31-46

Atmospheric Turbulence Compensation (ATC) methods have long been used to remove atmospheric turbulence effects from optical imaging systems. Traditional ATC methods were predominantly implemented in software and were generally slow with ATC taking hours to days for images with average number of pixels. Recently, the Well Optimized Linear Finder (WOLF) methodology has been developed for high-speed, diversity-based and phase-dominant, transfer function estimation problems across the electromagnetic and acoustic spectrum. Consequently, the WOLF paradigm has direct relevance to ATC problems for imaging systems. The WOLF methodology is orders of magnitude faster and more accurate than traditional, iterative ATC methods. The WOLF algorithm applies to diversity-based ATC methods and similarly can be implemented largely in software. In this study we use complexity analysis to theoretically compare the WOLF paradigm to traditional diversity-based ATC methods and validate our theoretical results using computer simulation. We analyze the computational complexity by using order analysis and also by comparing the number of elementary operations of a traditional ATC method with the new WOLF paradigm. Both approaches show that the WOLF paradigm is orders of magnitude faster than traditional ATC methods on conventional laptop and desktop computers. The WOLF paradigm can also be implemented using parallel processing technology such as using the Graphical Processing Unit (GPU) on standard computers/laptops, or Field Programmable Gated Arrays (FPGAs), and is expected to exceed the computational speed performance of traditional ATC methods on comparable single processor or parallel processing devices. Computer timing and scaling simulations were run on a 2014 MacBook Pro Laptop with a 2.8 GHz Quad-Core Intel Core i7 processor, 16 GB 1600 MHz DDR3 memory, and a NVIDIA GeForce GT 750M 2 GB graphics card and confirm our theoretical results from small 5×5 entrance pupil samples up to 1024×1024 samples.

INTRODUCTION

In the field of optical imaging, Atmospheric Turbulence Compensation (ATC) methods, such as phase diversity have long been used to remove atmospheric turbulence effects from optical imaging systems. Traditional ATC methods were predominantly implemented in software and used iterative 2-D Fourier transforms in a sequential error-reduction methodology which were generally slow with ATC taking hours to days for images with average number of pixels.

Recently, the Well Optimized Linear Finder (WOLF) methodology has been developed for high-speed, diversity-based and phase-dominant, transfer function estimation problems across the electromagnetic and acoustic spectrum. The WOLF methodology is orders of magnitude faster and more accurate than traditional, iterative ATC methods.

In this study, we use time complexity theory to compare theoretically the run time between the WOLF methodology and traditional diversity-based methods. We first analyze the functional flow block diagram (FFBD) used in a traditional, representative, Phase Diversity ATC methodology. Then, we use this result to find which operations are the most computationally complex and dominant operations in the traditional Phase Diversity ATC methodology. We then repeat this process for the WOLF methodology and compare the time complexity of the dominant operations in each methodology. The result provides the means to compare which methodology is less computationally complex and theoretically faster. We follow the theoretical comparison with computer simulation results and conclusions

TIME COMPLEXITY

In computer science, the time complexity is the computational complexity that describes the amount of computer time it takes to run an algorithm. Time complexity is commonly estimated by counting the number of elementary operations performed by the algorithm, supposing that each elementary operation takes a fixed amount of time to perform. Using the time complexity theory, we can often describe the run time of an algorithm merely by inspecting the algorithm's overall structure [5]. If we want to estimate the time complexity of an algorithm, we need to find the dominant operations in the algorithm, and analyze the time complexity of the dominant operations, while ignoring other non-significant operations [3, 4, 5]. The time complexity of the dominant operation can represent the time complexity of the entire algorithm. In the next section, we provide some background on ATC methods that employ diversity such as phase diversity.

Traditional Phase Diversity ATC Methodology

A linear, shift invariant imaging model can be applied to a wide variety of incoherent imaging problems [1, 7, 11, 12, 15]. The theoretical and mathematical model for an incoherent imaging system is given by,

$$\vec{i}(\vec{x}) = \vec{o}(\vec{x}) * |\vec{h_i}(\vec{x})|^2, \tag{1}$$

where $o(\vec{x})$ is the un-aberrated radiant emittance (object brightness function), $h_i(\vec{x})$ is the impulse response, $|h_i(\vec{x})|^2$ is the imaging system's point spread function (PSF) and $i(\vec{x})$ is the aberrated image due to atmospheric and optical imaging system effects, $(\vec{x})$ is a 2D position vector and the asterisk represents 2D spatial convolution. By taking the 2D Fourier transform of Equation (1), we can get Equation (2) which is a fundamental result for linear imaging systems,

$$I(\vec{f}) = O(\vec{f})\,\mathcal{H}(\vec{f}). \tag{2}$$

Here, $I(\vec{f})$ is the image spectrum, $O(\vec{f})$ is the object spectrum, and $\mathcal{H}(\vec{f})$ represents the optical transfer function (OTF), and $\vec{f}$ is a 2D spatial frequency variable. The Generalized Pupil Function (GPF) is given by,

$$(\vec{x}) = (\vec{)}^{j\theta(\vec{x})}, \tag{3}$$

where $A(\vec{x})$ is an amplitude function, $\theta(\vec{x})$ is the atmospherically induced phase aberration realized at spatial coordinate $(\vec{x})$ in the entrance pupil of the imaging system.

In diversity-based traditional ATC methods, a common approach is to insert some sort of known diversity into the system and simultaneously capture the original image and the diversity image

$$W_{pd}(\vec{x}) = A(\vec{x})e^{j(\theta(\vec{x})+\theta_{pd}(\vec{x}))}. \tag{4}$$

Here, $(\vec{)}$ is the phase diverse GPF, $\theta_{pd}(\vec{x})$ is a prior known, and introduced, phase diversity.

In the traditional Phase Diversity ATC methodology, we use a suitable basis set like the Zernike polynomials initially to generate an entrance pupil plane-phase estimate. The process for estimating the OTF is [2]:

1. Using a suitable basis set like the Zernike polynomials initially to generate an entrance pupil plane-phase estimate. This is done by just initially guessing the phase, for example, that all phase values are Zero;
2. Forming the generalized pupil function;
3. Zero-packing the GPF for sampling reasons in preparation of generating an OTF estimate;
4. Forming the impulse response;
5. Determining the PSF estimate by point-wise taking the magnitude squared of the result of step 4 above;
6. Form the OTF estimate and diversity OTF estimate;
7. After forming both the OTF and diversity OTF estimates, applying a suitable error metric such as the Gonsalvez error metric [8] and possibly some constraints to determine the instantaneous squared error at each spatial frequency location in the OTF;
8. Summing the squared errors at each spatial frequency and dividing by the total entrance pupil plane points to determine the total aperture averaged mean squared phase error for the initial entrance pupil plane phases;
9. Changing the weights on the Zernike polynomials in a methodical manner to come up with a new entrance pupil plane phase estimate;
10. Repeating steps 2 through 8 to generate a new error estimate;
11. Comparing the new error estimate to the old estimate and keeping the phase estimates associated with the lowest error;
12. Continuing to execute steps 10 and 11 until the error is minimized and the corresponding best OTF estimate is obtained.

In the next section we apply Time Complexity analysis to a representative, traditional diversity-based ATC methodology.

Analysis of the Time Complexity for the Traditional Phase Diversity ATC Methodology

We can draw the FFBD (Figure 1) of the traditional Phase Diversity ATC methodology, and find which operation is the dominant operation in each part of the FFBD. Assume we have a square entrance pupil, the total number of samples in the entrance pupil $N_p = n \times m$, where n is the number of entrance pupil plane points in the x-direction and m is the number of entrance pupil

plane points in the y-direction. After zero-packing to prevent aliasing, the minimum number of points on the OTF is required to be $N_H = N_{Hx} \times N_{Hy}$ where N_{Hx} is the number of required OTF points in the x-direction and N_{Hy} is the number of required OTF points in the y-direction. Mathematically, $N_{Hx} = 2n - 1$, and $N_{Hy} = 2m - 1$. To comply with the 2D Fast Fourier Transform requirements, we increase the number of points in each direction to the next power of 2 by,

$$N_{P2H} = (2^{[log_2(2n-1)]}) \times (2^{ceil[log_2(2m-1)]}), \quad (5)$$

where N_{P2H} is the total zero-packed number of points in the OTF (and image) in the x and y directions.

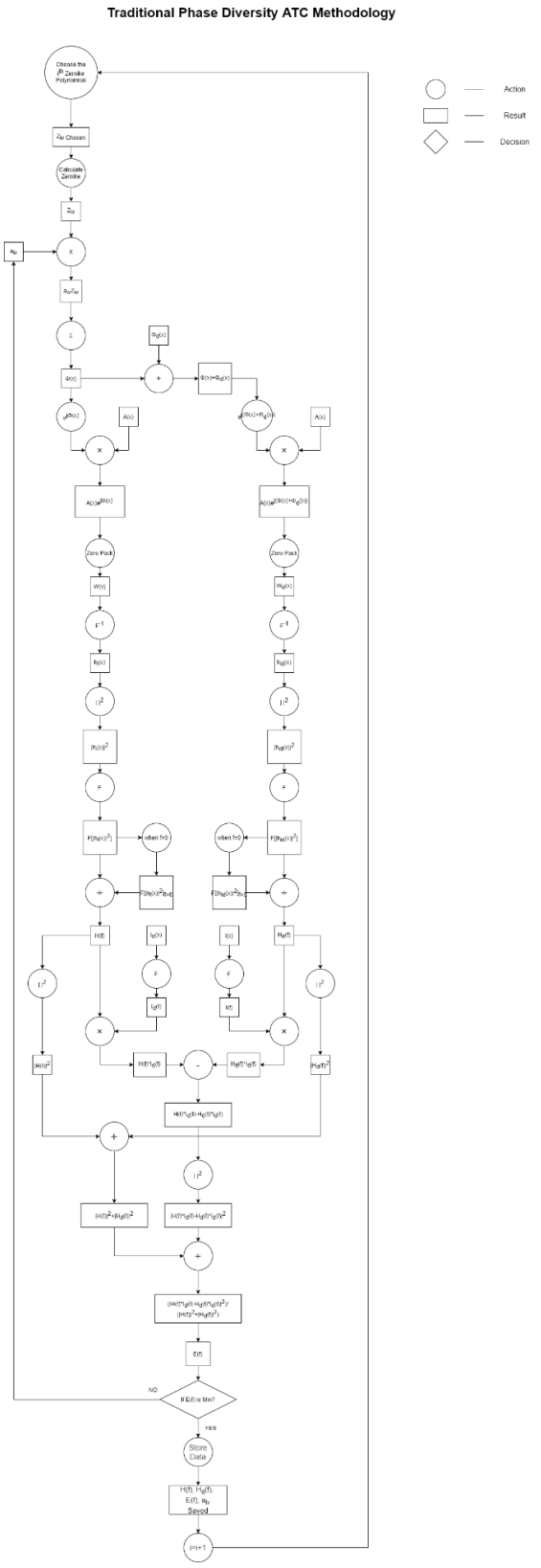

Figure 1: Functional Flow Block Diagram of Traditional Phase Diversity Methodology

Zernike Polynomials

In imaging systems, Zernike polynomials have been widely used to estimate atmospheric aberrations. The general form of an expansion of phase aberrations in an optical wave front, $(\vec{x})$ is

$$T(\vec{x}) = \sum_{i=1}^{N} a_{iv} Z_i \,. \tag{6}$$

Here, Z_i is the i^{th} Zernike polynomial, a_{iv} is the v^{th} weighting coefficient corresponding to the i^{th} Zernike polynomial in the range $[-\pi, \pi]$. We only calculate the first 9 Zernike polynomials, because 9 Zernike polynomials in the entrance pupil plane of the imaging system can represent a substantial amount of atmospheric phase errors. Note that additional Zernike terms can be readily added if required for higher phase estimation accuracy. In Table 1, we summarize the first 9 Zernike expressions. Note that they are functions of position in the entrance pupil plane. We divided the Zernike weights into 1000 increments in the range of $[-\pi, \pi]$, where a_{iv} is the v^{th} value in the set of Zernike weights. Therefore, $i \in [1, 9], a \in [1, 1000]$.

i	Zernike polynomial
1	1
2	$2rcos\theta$
3	$2rsin\theta$
4	$3.464r^2 - 1.732$
5	$2.449r^2sin2\theta$
6	$2.449r^2cos2\theta$
7	$(8.485r^3 - 5.657r)sin\theta$
8	$(8.485r^3 - 5.657r)cos\theta$
9	$2.828r^3sin3\theta$

Table 1: First 9 Zernike polynomials

The FFBD shown in Figure 2 is related to determining Zernike Basis functions. Therefore, from Figure 2 and the table, we can see that time complexity operations include add, minus, multiply, square, cube, sin and cos.

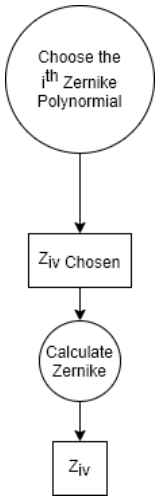

Figure 2:
Functional Flow Block Diagram for determining specific candidate Zernike basisfunctions.

Add, minus, multiply are elementary operations, and the square and cube can be treated as multiplies. Consequently, the trigonometric functions are the most complicated operations and are

the dominant operations in Figure 2.

Before Zero-Packing

The FFBD before the zero-packing operation is shown in Figure 3. We take 1000 equal distant points in the range $[-\pi, \pi]$, to set 1000 different a_{iv} weights. We need to calculate the first 9 Zernike polynomials, so the steps after defining the Zernike polynomials need to be executed 9000 times. Before the zero-packing operation, from the FFBD in Figure 3, we can see the operations have adds, multiplies and complex exponential functions. In these operations, only the complex exponential functions are the non-elementary operations. Therefore, the complex exponential functions are the dominant operations. Since the complex exponential functions dominate, we can safely ignore the elementary operations because they are less computationally complex.

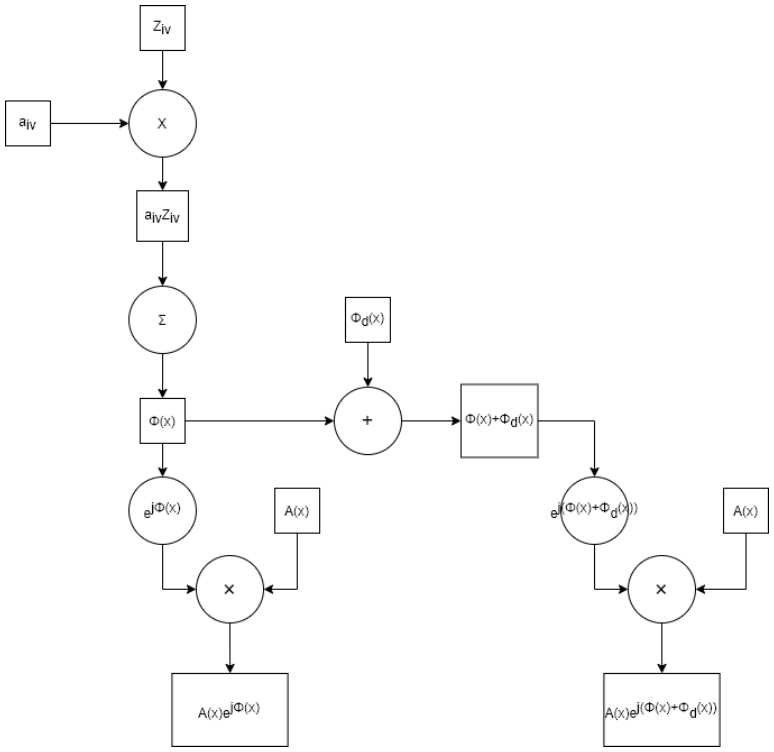

Figure 3: Functional Flow Block Diagram before Zero-Packing

After Zero-Packing

The FFBD after zero-packing is shown in Figure 4. After zero-packing, the number of image points will scale as N_{P2H}. After zero-packing, from the FFBD in Figure 4, we can see the operations have adds, multiplies, division, zero-packing, modulus squared, 2D Fourier Transform and inverse 2D Fourier Transform operations. Besides the elementary operations, we still have zero-packing, modulus squared, 2D Fast Fourier Transform and inverse 2D Fast Fourier Transform, as the more complex functions. We will analyze the time complexity of these non- elementary operations.

The zero-packing process is to avoid aliasing effects, ensuring sufficient sample points are collected across the entrance pupil plane (collecting aperture of the telescope). The number of samples will change from N_P to N_{P2H}. We can treat the zero-packing process as not computationally significant in the traditional Phase Diversity ATC methodology. For the modulus squared, if the number is an integer or a real number, the algorithm is very straight forward,

Therefore, from Equation (8), it can be seen that the time complexity of the modulus squared is $(_{2H})$. For the 2D Fast Fourier Transform, the time complexity is $(_{2H}\ log\ N_{P2H})$ [3]. Therefore, the 2D Fast Fourier Transform is the dominant operation in the operations of Figure 4.

When considering the whole traditional Phase Diversity ATC methodology, the dominant operations are trigonometric functions, complex exponential functions, the 2D FFT and 2D IFFT. We will analyze these operations in the next section.

$$|x|^2 = x^2, \tag{7}$$

If the number is a complex number,

$$|z|^2 = |a + bi|^2 = |\sqrt{a^2 + b^2}|^2 = (\sqrt{a^2 + b^2})^2 = a^2 + b^2, \tag{8}$$

Further Analysis

For the complex exponential functions， exp (jx), this is not a function of N_{P2}, but rather a matter of convergence. We therefore need an alternate strategy to analyze its time complexity. One solution is to use precision arguments to provide insight to the convergence of complex exponential functions. We discuss this next.

Define β^k as the arbitrary precision of the functions, where β is the base of the precision, and k is the number of base β digits in an integer. As an example, if we use double-precision floating-point, the required precision is 2^{53}, where the base $\beta = 2$, $k = 53$. The time complexity of the 2D FFT is $(klogkloglogk)$ [3, 14]. From Euler's formula $e^{jx} = \cos(x) + jsin(x)$, we see that $\sin(x)$, $\cos(x)$, exp (jx) has the same time complexities, which is $O(M(k)log^2k)$ [9], where $M(k)$ represents the time to multiply k-bit integers. In the polynomial case, we assume that the cost of multiplying coefficients is constant. In time complexity theory, the constant (k) can be eliminated [4].

In Figure 5, we draw the time complexity plot of the 2D FFT and complex exponential functions. We can see when $k > 20$, the time complexity of the 2D FFT is much larger than for the complex exponential functions. In evaluating both the traditional Phase Diversity ATC methodology and the WOLF methodology, we assume double-precision floating-point, so that $k = 53$, from Figure 5 we see that the 2D FFT is the dominant operation in the traditional Phase Diversity ATC methodology.

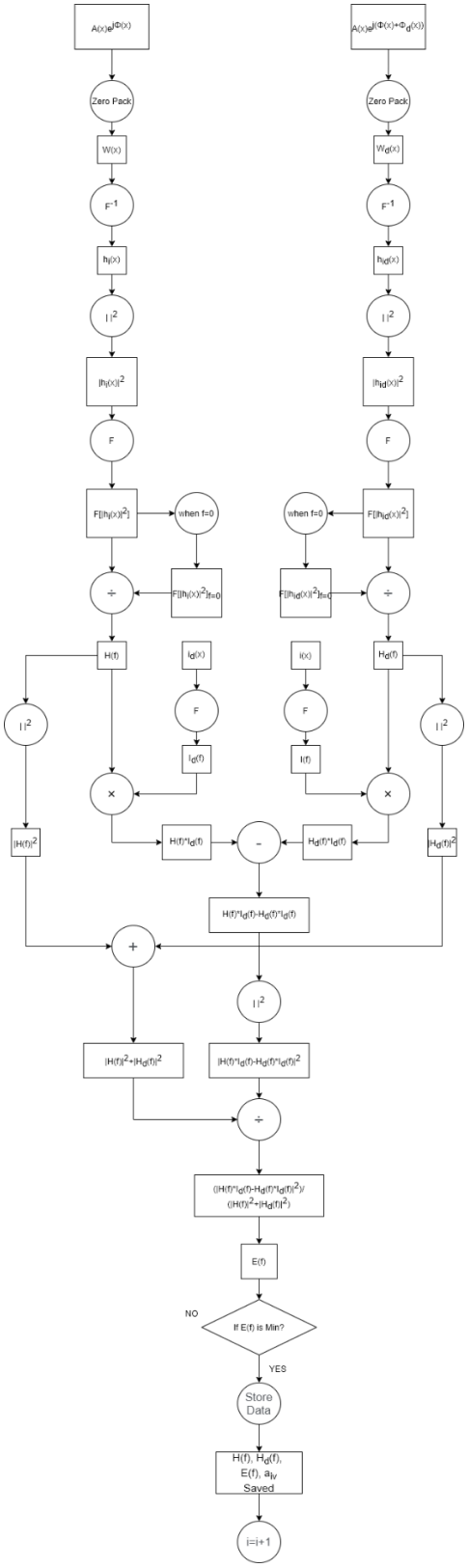

Figure 4: Functional Flow Block Diagram after Zero-Packing

Furthermore, for the entire traditional Phase Diversity ATC methodology, if the image size is 256 by 256 pixels, the total number of image samples will be 65536. For the upper bound, the whole process will iterate 1000 times for each Zernike basis function, and we use just 9 Zernike basis functions. We will execute the 2D FFT 7 times and the complex exponential functions 2 times in each loop. Trigonometric functions are only calculated when determining Zernike polynomials and will not be part of the iterative calculations, since the run times for the trigonometric functions are much smaller than the 2D FFT and the complex exponential functions.

Summarizing, the entire traditional Phase Diversity ATC method will run the 2D FFT 4.13×10^9 times, complex exponential functions 1.18×10^9 times when the image size is 256 by 256 pixels. Therefore, the 2D FFT not only has the highest value of time complexity, but also is the most executed function in the entire traditional Phase Diversity ATC method. We note that the 2D FFT is the dominant operation in the traditional Phase Diversity ATC method.

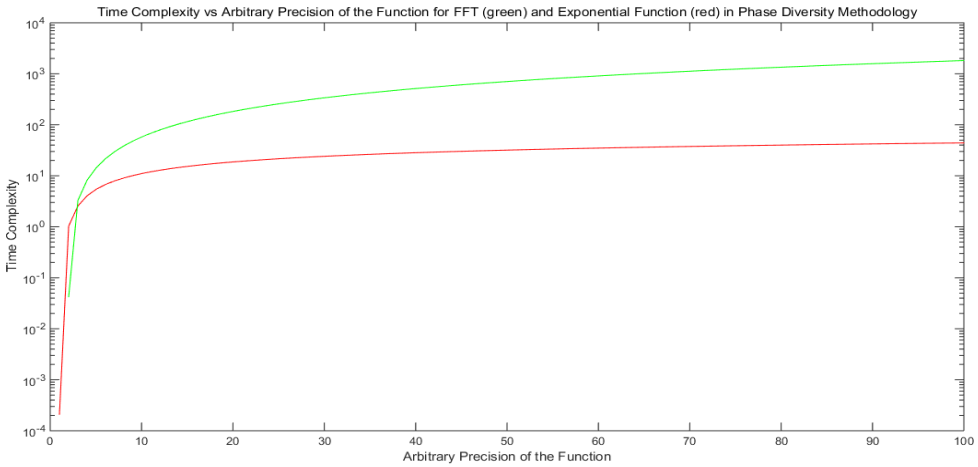

Figure 5: Time Complexity vs Arbitrary Precision of the Function for 2D FFT and Complex Exponential Function in Phase Diversity Methodology

WOLF Methodology

The WOLF methodology FFBD is shown in Figure 6. We show the complete WOLF methodology FFBD as a reference for subsequence figures. We separate the FFBD in several different sections to analyze the time complexity.

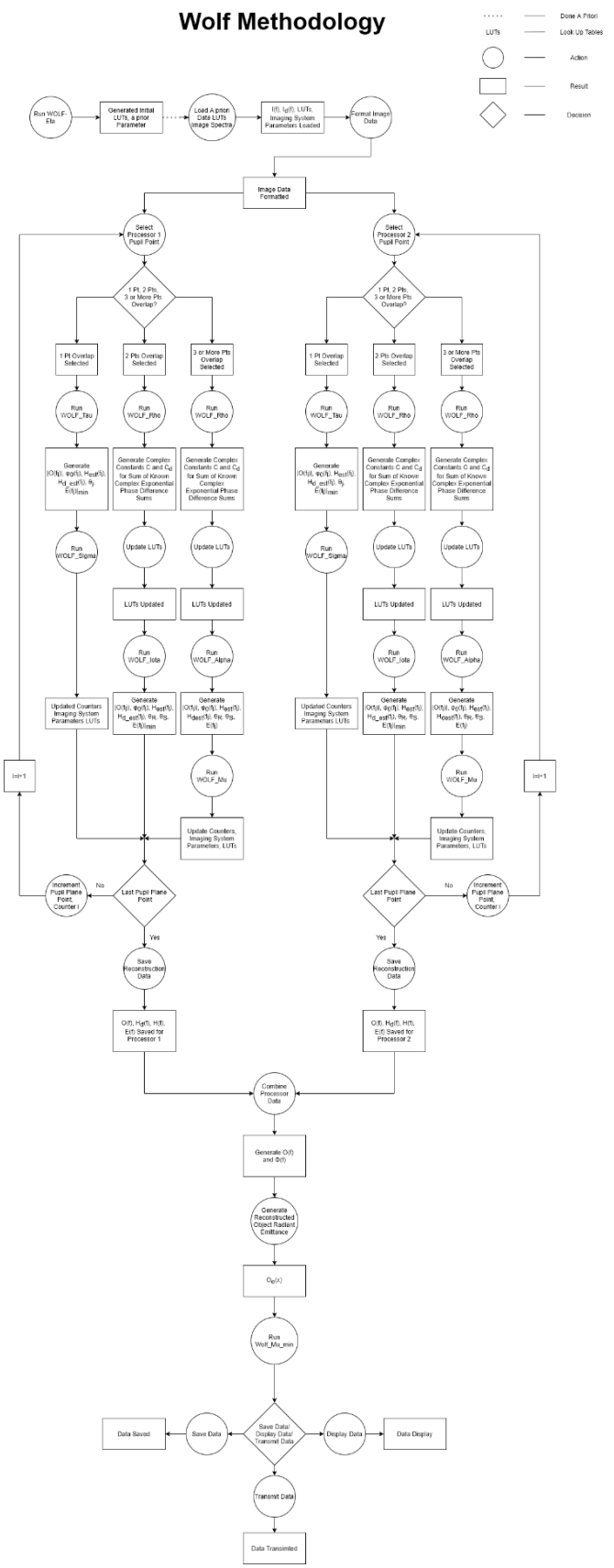

Figure 6: Functional Flow Block Diagram of WOLF Methodology

Image Data Formatting

In Figure 7, we show the operations in the WOLF methodology related to image data formatting. All the operations in this part are used to format the image data, so there are no time complexity significant operations. Consequently, we can safely ignore the time complexity of the operations shown in Figure 7.

Figure 7: Functional Flow Block Diagram of Image Data Formatting

Overlap Scenario

There are three fundamental kinds of overlap scenarios in the WOLF methodology: One Point Overlap, Two Point Overlap and Three or More Point Overlap. The FFBD in Figure 8 shows the critical operations in the WOLF paradigm. For the overlap scenarios, the One-Point overlap is calculated by WOLF_Tau, the Two-Point overlap is calculated by WOLF_Iota, the Three or More Point overlap is calculated by WOLF_Rho, WOLF_Alpha, and WOLF_Mu. If we assume the entrance pupil plane aperture has $n \times m$ samples, the number of required point calculations in the WOLF methodology with a single processor is $\frac{n \times m}{2}$, and $\frac{n \times m}{4}$ for a single parallel processor.

As a representative example, assume that we have a square entrance pupil plane aperture, with samples $n = m$, for $n = m \geq 8$, with a computing system using a single parallel processor, the number of points calculated by the One-Point overlap is 1, the number of points calculated by the Two-Point overlap is 2, the number of points calculated by the Three or More Point overlap is $\frac{n \times m}{4} - 3$. Consequently, for a large number of entrance pupil plane aperture samples, the number of points calculated by the Three or More Point overlap is much larger than the One-Point overlap and the Two-Point overlap. Therefore, the Three or More Point Overlap path in Figure 6 will be the dominant path in the WOLF methodology. We therefore focus on the case for the Three or More Point Overlap.

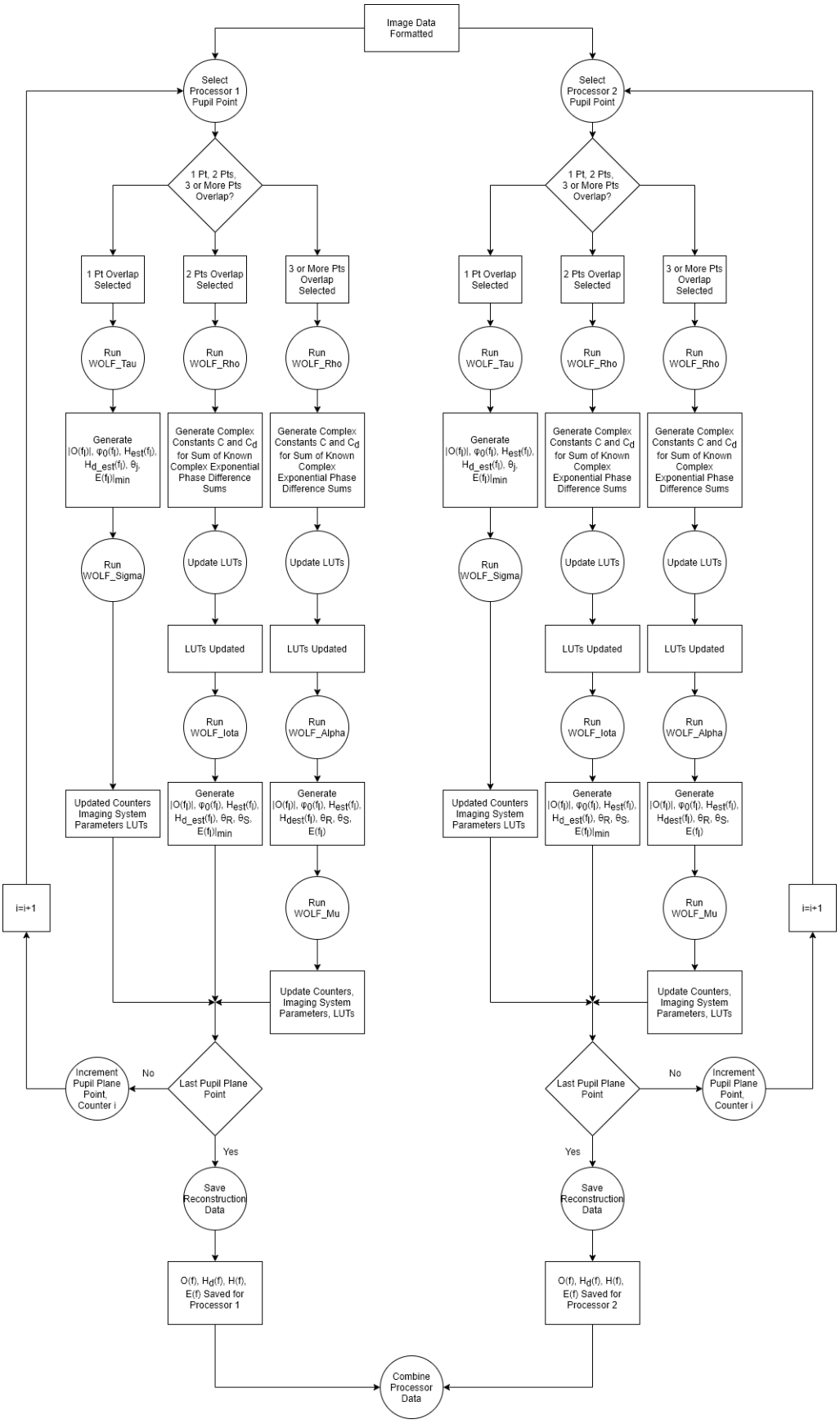
Image Data Formatted
Select Processor 1 Pupil Point
Select Processor 2 Pupil Point
1 Pt, 2 Pts, 3 or More Pts Overlap?
1 Pt Overlap Selected
2 Pts Overlap Selected
3 or More Pts Overlap Selected
Run WOLF_Tau
Run WOLF_Rho
Generate |O(fi)|, Φ0(fi), Hest(fi), Hd_est(fi), θj, E(fi)|min
Generate Complex Constants C and Cd for Sum of Known Complex Exponential Phase Difference Sums
Run WOLF_Sigma
Update LUTs
LUTs Updated
Run WOLF_Iota
Run WOLF_Alpha
Generate |O(fi)|, Φ0(fi), Hest(fi), Hd_est(fi), θR, θS, E(fi)|min
Generate |O(fi)|, Φ0(fi), Hest(fi), Hdest(fi), θR, θS, E(fi)
Updated Counters Imaging System Parameters LUTs
Run WOLF_Mu
Update Counters, Imaging System Parameters, LUTs
Last Pupil Plane Point
No
Yes
Increment Pupil Plane Point, Counter i
i=i+1
Save Reconstruction Data
O(f), Hd(f), H(f), E(f) Saved for Processor 1
O(f), Hd(f), H(f), E(f) Saved for Processor 2
Combine Processor Data

Figure 8: Functional Flow Block Diagram of Entrance Pupil Plane Overlap Scenario

For the Three or More Point Overlap scenario, there are four operations: update Look up Tables (LUTs), run WOLF_Rho, run WOLF_Alpha, and run WOLF_Mu. For the update LUTs operations, only data transfers occur and so we don't need to estimate this time complexity. For WOLF_Mu, this algorithm adjusts the pointers and counters, and provides diagnostics. The main parts of the WOLF paradigm needed by the time complexity analysis for the Three or More Point Overlap scenario are WOLF_Rho, WOLF_Alpha and WOLF_Mu.

For WOLF_Rho, this algorithm is used to calculate complex constants, which are used in the WOLF_Alpha algorithm. For WOLF_Alpha, this algorithm determines the needed entrance pupil plane phases and OTF parameters for the image and diversity image. Within the WOLF_Alpha algorithm we have the following basic operations: addition, multiplication, division, modulus and complex exponential functions. The non-elementary operations are modulus and complex exponential functions. We previously analyzed the modulus and complex exponential functions, and from the time complexity theory, complex exponential functions are the dominant functions in WOLF_Alpha.

Data Reconstruction

In Figure 9, the operations are all about data transmission, display, saving and reconstructing the data. There are no complexity analysis relevant calculations in this section. Operations in the FFBD are only involved manipulating the data. We can ignore this part of the FFBD when calculating the time complexity.

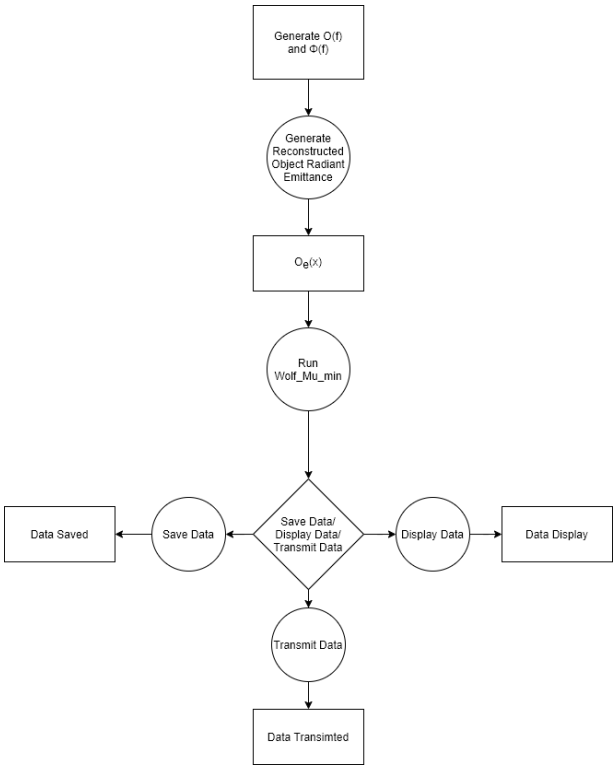

Figure 9: Functional Flow Block Diagram of Data Reconstruction

In conclusion, the dominant operation in the entire WOLF methodology is the complex exponential functions. The time complexity of the complex exponential function is $((k)^{2}k)$.

CONCLUSION

By analyzing the traditional Phase Diversity ATC methodology, the dominant operation was found to be the 2D FFT, and the time complexity is $(klogkloglogk)$. The dominant operation in the WOLF methodology is the complex exponential function with time complexity $((k)^2 k)$.

We determined that the time complexity of the 2D FFT is much larger than the complex exponential function that dominates in the WOLF methodology. When we use double-precision floating-point to estimate the OTF, it requires that the precision is 2^{53}. The time complexity of the 2D FFT is much larger than the complex exponential function. Therefore, we expect the WOLF methodology to be computationally faster than the traditional Phase Diversity ATC methodology. In the next section, we present our simulated results.

SIMULATION RESULT

In the traditional Phase Diversity ATC methodology, for estimations of the time complexity, the whole process will iterate 1000 times for each Zernike basis function, and we use the first 9 Zernike basis functions to execute the 2D FFT 7 times for every single aperture sample in each loop. Therefore, we can calculate the 2D FFT run time for different sizes of the aperture in the traditional Phase Diversity ATC methodology, and compare the run time with the Three or More Point Overlap path in the WOLF methodology. Table 2 shows the run time of the traditional Phase Diversity ATC methodology and the Three or More Point Overlap path of the WOLF methodology using a parallel processor.

Number of Entrance Pupil Samples	Run Time of Phase Diversity ATC Method(s)	WOLF_Alpha (s)	WOLF_Mu (s)	WOLF_Rho (s)	Total Run Time of WOLF Alpha Mu and Rho (s)
5×5	6.1152E+00	8.1331E-04	5.0691E-03	1.2779E-03	7.1603E-03
7×7	6.1152E+00	1.5941E-03	9.9355E-03	2.5046E-03	1.4034E-02
9×9	8.9654E+00	2.6351E-03	1.6424E-02	4.1403E-03	2.3199E-02
15×15	8.9654E+00	7.3198E-03	4.5622E-02	1.1501E-02	6.4443E-02
31×31	1.3144E+01	3.1264E-02	1.9486E-01	4.9122E-02	2.7524E-01
63×63	4.8324E+01	1.2912E-01	8.0477E-01	2.0288E-01	1.1368E+00
127×127	2.0854E+02	5.2472E-01	3.2704E+00	8.2443E-01	4.6195E+00
255×255	1.3791E+03	2.1154E+00	1.3185E+01	3.3238E+00	1.8624E+01
511×511	5.1743E+03	8.4949E+00	5.2946E+01	1.3347E+01	7.4788E+01
1023×1023	1.3239E+04	3.4046E+01	2.1220E+02	5.3493E+01	2.9974E+02

Table 2: Timing Results Supporting Complexity Analysis for WOLF Paradigm

We show the run time results graphically in Figure 10. From Figure 10, we can see the WOLF methodology is computationally about two orders of magnitude faster than the 2D FFT in the traditional Phase Diversity ATC methodology. If we use the number of elementary operations to evaluate the traditional Phase Diversity ATC methodology and the WOLF methodology using a parallel processor, the results are shown in Figure 11. Figure 11 shows the number of elementary operations in the traditional Phase Diversity ATC methodology is about two orders of magnitude larger than the WOLF methodology. Therefore, we see good agreement between Figure 10 and 11.

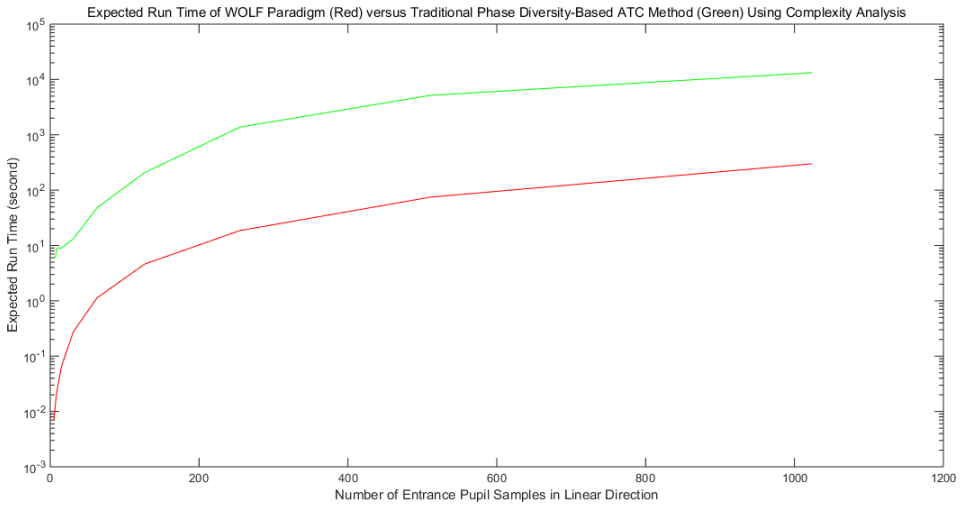

Figure 10: Comparison of Theoretical Run Times for WOLF Methodology versus Representative Traditional ATC Methodology

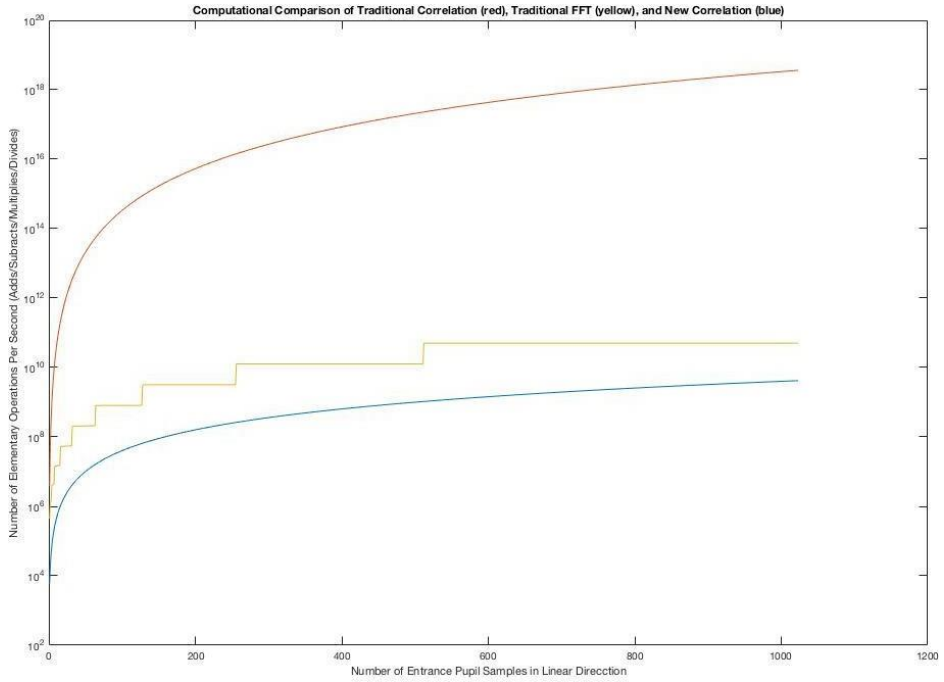

Figure 11: *Comparison of the Number of Elementary Operations for WOLF Methodology versus Representative Traditional ATC Methodology*

From Table 2, we can see that the total run time of WOLF_Alpha, WOLF_Mu and WOLF_Rho for 127×127 entrance pupil plane samples with parallel processing is 4.6195 seconds, which means the run time of a single processor system is about 9.2 seconds. This result matches our simulation result of the whole WOLF methodology run time for the 127×127 entrance pupil plane samples with a single processor of 8.2 seconds. The standard deviation of the theoretical timing results is 4.5824×10^{-4} which results in the expected run time in the range of 5.54 seconds to 12.94 seconds, and our simulation result of 8.2 seconds is in this range. Consequently, our theoretical complexity analysis-based results match our simulated timing results within one standard deviation range and are considered a good match.

REFERENCE

1. Roggemann, Michael C., and Byron M. Welsh. *Imaging through turbulence*. CRC press, 2018.
2. W. W. Arrasmith, "High-speed Diversity-based Imaging Method for Parallel Atmospheric Turbulence Compensation," U.S. patent number: US 8,447,129 B2, May 21, 2013.
3. Brent, Richard P., and Paul Zimmermann. *Modern computer arithmetic*. Vol. 18. Cambridge University Press, 2010. P163.
4. Fleck, Margaret M. "Building Blocks for Theoretical Computer Science (Version 1.3)." (2013).
5. Cormen, Thomas H., et al. *Introduction to algorithms*. MIT press, 2009.
6. Goodman, Joseph W. *Statistical optics*. John Wiley & Sons, 2015.
7. Goodman, Joseph W. *Introduction to Fourier optics*. Roberts and Company Publishers, 2005.
8. Gonsalves, Robert A. "*Phase retrieval and diversity in adaptive optics.*" *Optical Engineering* 21.5 (1982): 215829.
9. Brent, Richard P. "The complexity of multiple-precision arithmetic." *The complexity of computational problem solving* (1976): 126-165.
10. Sanders, Jason, and Edward Kandrot. *CUDA by example: an introduction to general-purpose GPU programming*. Addison-Wesley Professional, 2010.
11. D. L. Fried, "Optical Resolution through a Randomly Inhomogeneous Medium for Very Long and Very Short Exposures," *J. Opt. Soc. Am*., Vol 56, p1372-1379.
12. R. K. Tyson, *Principles of Adaptive Optics*, Academic Press, Boston, 1991.
13. Jin, Haimin, Duncan S. Wong, and Yinlong Xu. "Complexity Analysis of a Fast Modular Multiexponentiation Algorithm." *IACR Cryptol. ePrint Arch*. 2008 (2008): 210.
14. Schönhage, Arnold and Strassen, Volker. 1971. Schnelle Multiplikation großer Zahlen. *Computing*, 7, 281–292.
15. D. Korff, "Analysis of a method for obtaining near-diffraction-limited information in the presence of atmospheric turbulence," *J. Opt. Soc. Am*., Vol. 63, p971-980, 1973.